Received: 24 March 2021 | Revised: 23 June 2021 | Accepted: 6 July 2021

DOI: 10.1049/elp2.12113

IET Electric Power Applications

The Institution of Engineering and Technology WILEY

ORIGINAL RESEARCH PAPER

Power losses in the three-phase three-limb transformer due to common and differential mode of dc-bias

Wei Wang[1] | **Arne Nysveen**[1] | **Niklas Magnusson**[2]

[1]Electric Power Department, Norwegian University of Science and Technology, Trondheim, Norway

[2]SINTEF Energy Research, Trondheim, Norway

Correspondence

Wei Wang, Electric Power Department, Norwegian University of Science and Technology, Elektro E/F, Gløshaugen, O. S. Bragstads plass 2, 7491 Trondheim, Norway.
Email: weiwan@ntnu.no

Funding information

Research Council of Norway, Grant/Award Number: Norges Forskningsråd: 255178

Abstract

Geomagnetically induced currents (GICs) and the converter modulation effect are the two main causes for dc magnetisation in power transformers. It is well known that a small dc-bias can saturate a large transformer and thereby generate high unbalanced magnetising currents, imposing a serious risk of excessive power losses and local overheating. Magnetising currents due to GIC phenomena have been studied extensively, whereas studies on converter related dc-bias are few. In particular, a discussion on loss characteristics related to converter modulation lacks. In this study, the dc-bias of common mode and differential mode in a three-phase, three-limb transformer is investigated experimentally. Additionally, to interpret the physical phenomena, the system was modelled using the finite element method. The results revealed that the power losses are significantly influenced by the dc current direction, arrangement of the structural parts, and the method of winding connection.

1 | INTRODUCTION

DC magnetisation due to geomagnetically induced currents (GICs) [1] and converter modulation [2] may cause core saturation in grid transformers. The dc magnetisation yields high magnetising currents, which increase the noise level in the core and create local hotspots in the winding terminal and in iron structural parts such as the tank and the flitch plates [3, 4]. In the worst case, the generated heat can lead to the full failure of the transformer [5]. Moreover, the excessive magnetising current can deteriorate the performance of the power system [3]. For instance, it increases reactive power consumption, causes voltage instability [6], and the induced current harmonics may lead to incorrect operation of protection relays of HVDC systems, with the risk of tripping the entire transmission system [7].

The GIC originates from the interaction between the coronal mass ejections (CME) of the sun and the magnetosphere of the earth. The electrojet current (generated by the movement of the geomagnetic field relative to the conductive ionosphere) induces a longitudinal quasi-dc potential in series with the transmission lines, driving the flow of induced current, the GIC [3].

Another origin of dc-bias in power transformers is the modulation effect of power converters. When ac and dc transmission lines share the same corridor or even the same towers [8, 9], the ac line induces fundamental current in the dc lines by inductive coupling. Due to the switching operation of the power electronic converter, the fundamental signal on the dc side of the converter will then be transferred to the ac side and appear as dc-bias (and second order harmonic) [2].

The two mechanisms of dc magnetisation are illustrated in Figure 1. As depicted in the upper figure, the GIC flows through transmission lines and closes its path via the star connected windings of the grid transformer at the grounded neutral points. The GICs are oriented in the same direction in all three phases of the power lines, consequently, in the transformer windings. At very low frequencies (typically 0.01–0.5 Hz), the high-voltage network is essentially resistive. Considering equal resistance in the three phases, the magnitudes of GICs become identical in the three phases. Based on these factors, the GICs are common mode (CM) dominated and causes a zero-sequence magnetising current. In the lower figure, the inductive coupling due to power converter modulation is represented as two longitudinal voltage sources, which determines the dc current level in the transformer windings. Different from GICs, the sum of the dc currents appearing on the ac bus is zero (regardless of whether the transformer is

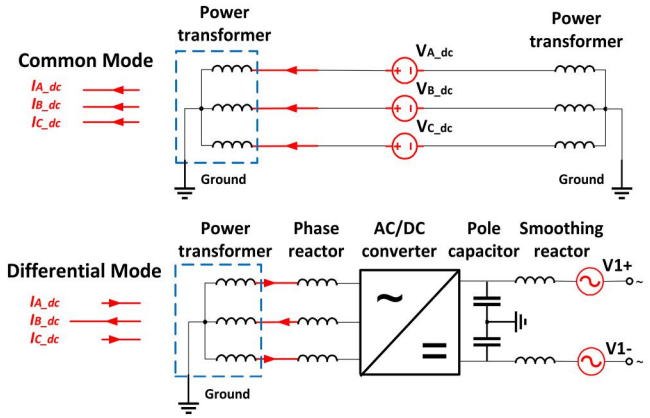

FIGURE 1 Illustration of dc-bias in a three-phase transformer. Upper: the dc-bias is generated by geomagnetic disturbances. The dc current in the transformer winding is of the common mode. Lower: the dc-bias is generated by the converter modulation effect. The dc current in the transformer winding is of the differential mode

grounded or not). Thus, they cannot be in the same direction. These currents are referred to as differential mode (DM).

The GIC phenomenon has been given significant attention and is investigated extensively for decades. The standard [3] has been widely used as a guideline to select or design power transformers subjected to GICs. As for the converter-related dc magnetisation, the physical consequence is similar to GICs in a single-phase transformer, which is used prevalently in large HVDC transmission projects. However, for HVDC projects with constraints in footprint of the converter station (e.g. offshore platform) [10, 11], three-phase transformers are sometimes preferred. In contrast to three single-phase units, where the electromagnetic field is isolated in each phase, the fluxes may interact within the core and structural parts in a three-phase transformer. Such interaction can be significant, particularly when flux saturates the core (due to dc currents).

As the dc currents are not identical in the three phases, it results in unsymmetrical magnetisation of the transformer core. The distribution of the dc voltages, u_{dc}, among the three phases depends on the phase difference, θ, between the induced voltage sources ($V_{1\pm}$ in Figure 1) and the switching operation of the converter [12]:

$$u_{dc} = \frac{mV_m}{2}\begin{bmatrix} \cos\theta \\ \cos\left(\theta - \frac{2\pi}{3}\right) \\ \cos\left(\theta + \frac{2\pi}{3}\right) \end{bmatrix} \quad (1)$$

where m is the modulation index and V_m is the peak voltage on the ac side of the converter. Since θ may take different values, the dc current distribution among the three phases can be largely different under different conditions. Table 1 defines four cases with θ varying from 0° to 150°. For comparison, the CM currents are also included.

The unsymmetrical magnetisation due to the DM dc current in the core may lead to a significantly different physical consequence in terms of losses, noise, and reactive power consumption, which makes the conclusions based on GICs invalid for a three-phase transformer. Understanding the behaviour of the three-phase transformer subjected to DM dc current becomes increasingly important due to recent HVDC projects and has not yet been addressed by any literature. In this study, we experimentally determine the power loss under different cases in a three-phase, three-limb transformer. The influence of dc current directions (CM and DM), the arrangement of the structural parts (tank, clamping plates) and delta connection on the losses are studied for the transformer. To interpret the results and explain the physical phenomena, the transformer is modelled using the finite element method.

TABLE 1 Examples of dc current ratios defined in each phase of the transformer windings for different phase differences

		DC current ratio in Phases A, B and C			
Mode	θ	I_{A_dc}	I_{B_dc}	I_{C_dc}	ΣI_{ABC_dc}
DM	0°	1	−0.5	−0.5	0
	60°	0.5	−1	0.5	0
	90°	$\sqrt{3}/2$	$\sqrt{3}/2$	0	0
	150°	$\sqrt{3}/2$	0	$\sqrt{3}/2$	0
CM	/	1	1	1	3

Abbreviations: CM, common mode; DM, differential mode.

2 | EXPERIMENTAL SETUP

2.1 | Test system

A 2.5-kVA three-phase three-limb transformer was used as the test object [12]. Both the primary and the secondary winding had 280 turns. The primary windings were connected (in star) to a three-phase power supply (the FPGA-based grid emulator, EGSTON®), with independently controllable phases. The secondary windings were connected in delta and a switch was used to allow the delta connection to be open (Figure 2). The grid emulator is a reconfigurable switching converter being able to emulate a power system as ac/dc sources (100 kVA, 400 V_{ac}/800 V_{dc}). The system offers a symmetric ac source with independent, controllable dc voltages. During the test, the dc currents can be tuned precisely to predesignated values, while the nominal ac voltage is maintained. The primary current and the voltage across each winding were measured in each phase of the transformer, and the measurements were incorporated into a high precision power analyser (YOKOGAWA WT3000), where the power losses were obtained.

The iron tank and the clamping plates (mild steel) can be disassembled such that the core loss, the stray losses of the tank, and the clamping steels can be separated. The height of the tank was adjustable, enabling the influence of geometry on stray loss to be further evaluated (Figure 3).

2.2 | Material measurement on the transformer

The data of the electric steel of a transformer is not always available for the user or even for the transformer designer, particularly when it needs a non-standardised test such as dc magnetisation. Although standardised material measurement methods for specific power loss [13, 14] as well as specially developed instruments for measurements of losses due to dc bias [15] exist, they cannot always be utilised. Comprehensive measurements are required to cover various combinations of ac and dc magnetomotive force (MMF) and, additionally, the availability of samples can be largely limited.

In a single-phase transformer, the magnetic properties of the electrical steel sheets can be characterised directly on the transformer (ac and dc fields can simultaneously be applied to the core as in [15]). However, for a three-phase transformer, such a standardised test is not applicable since the ac flux and dc flux have different paths in the yoke and the limbs, and the resultant total flux density is non-uniform in the core. In this section, we propose a simple method, which utilises a three-phase transformer to create a uniform flux distribution, and thereby enables a dc-bias test.

The winding connection is represented in the schematic diagram in Figure 4. The primary windings of Phases A and C (two side-limbs) of the transformer are connected in series and excited by a single-phase voltage source. The secondary windings of the Phases A and C are also connected in series and are used as a voltage measurement winding. In this way, the flux along the path l_c in Figure 4 becomes uniform. The ac flux and dc flux have the same path l_c. The flux path l_c comprises the side limbs and yokes. In principle, there is no flux flowing in the middle limb. To verify this, the induced voltage in the middle winding is monitored.

The measured specific power loss (loss per unit mass) versus ac flux density is shown in Figure 5. In all measurements, the induced voltage recorded in the middle limb was less than 1% of the voltage applied on the side limbs indicating that the power loss contributed by the middle limb was negligible. The specific power loss provided by the manufacturer is 1.35 W/kg at 1.0 T (red point in Figure 5), which agrees well with the measurements.

The example of magnetisation characterisation under the dc-bias is demonstrated in Figure 6, where the ac MMF of 1 per-unit (corresponding to 1.48 T) is superimposed with various dc MMFs.

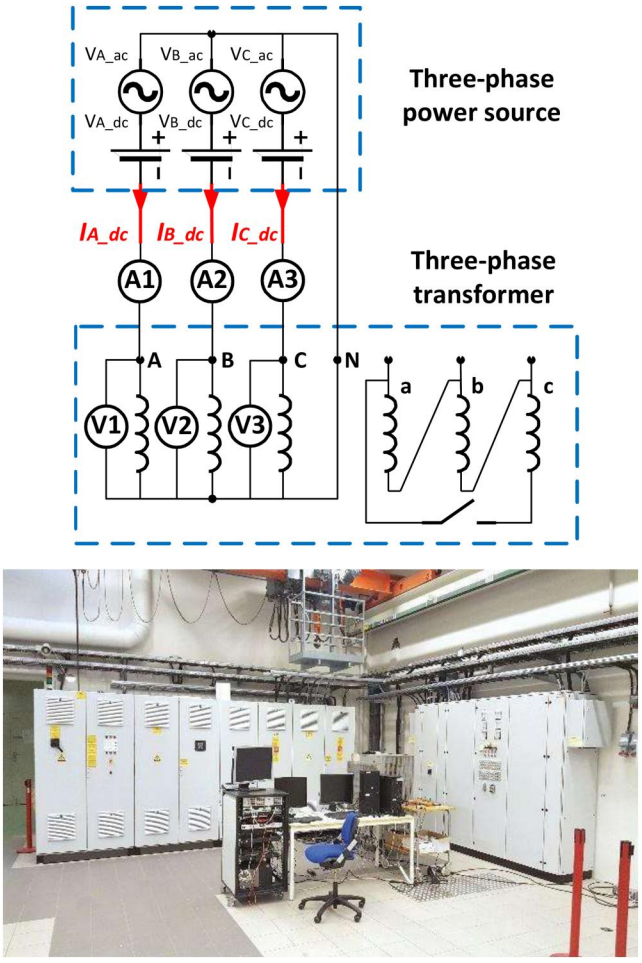

FIGURE 2 Test circuit (transformer winding connection and dc-bias implementation) and the EGSTON grid emulator (controllable three-phase voltage source) in the National Smart Grid Laboratory (NSGL), Norway

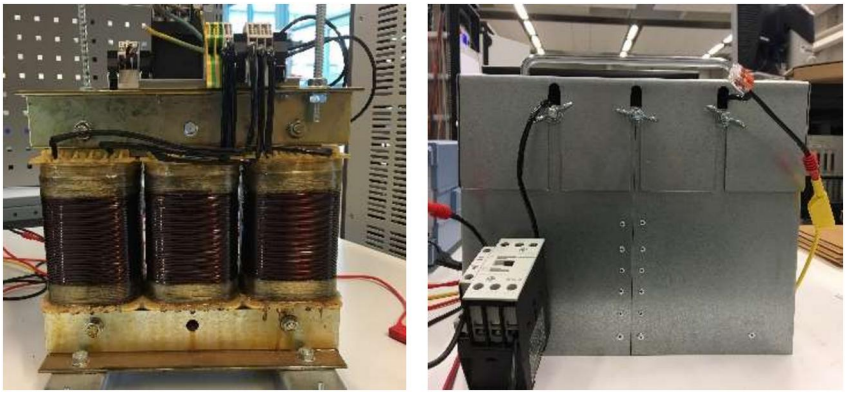

FIGURE 3 The 2.5-kVA three-phase three-limb transformer for dc-bias test

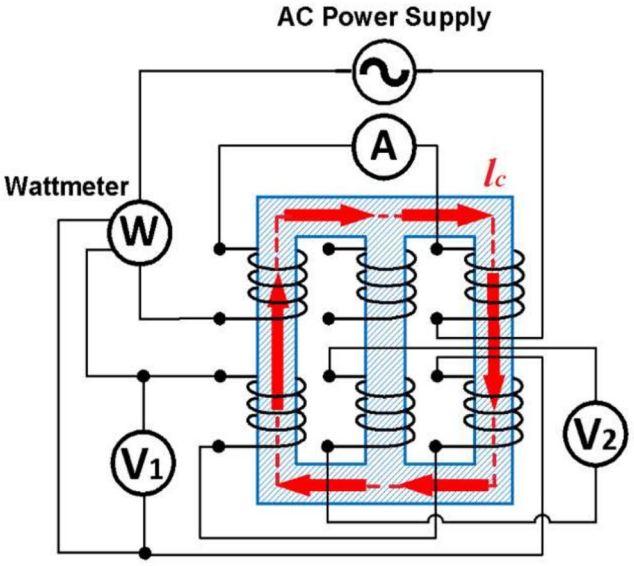

FIGURE 4 Schematic diagram for material magnetisation characterisation using a three-phase three-limb transformer. The dash line l_c and the red arrows represent the flux path in the transformer core. No flux passes through the middle limb. Note that the measurements are performed without tank and clamping steels

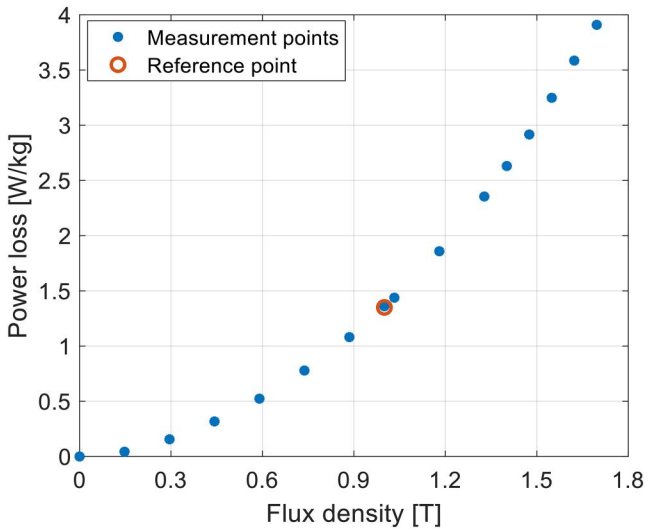

FIGURE 5 Measured specific power loss versus ac flux density. The reference point is given by the manufacturer

The half-cycle saturation is clearly observed from the *B-H* characteristic in Figure 6. Due to the dc-bias of the flux, the area of the hysteresis loop increases in one half-cycle and decreases in the other half-cycle. For high dc MMFs, the peak flux density exceeds the saturation point in one half-cycle. As a result, a moderate change of the hysteresis loss is expected with the increasing dc MMF. As shown in Figure 7, at low flux density (0.7 pu), the loss increases slightly with dc MMF and asymptotically approaches a constant value. At the nominal flux density (1 pu), the loss decreases slightly as dc MMF increases.

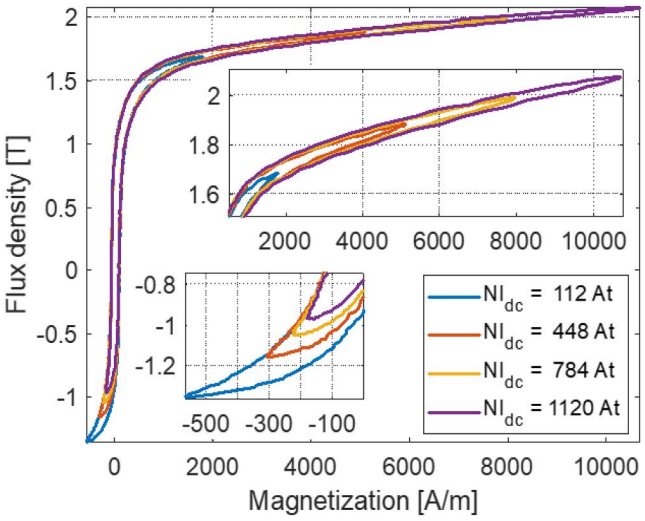

FIGURE 6 Magnetisation characteristic (B-H curve) under ac nominal MMF superimposed with multiple dc-bias levels

3 | FINITE ELEMENT MODELS FOR LOSS CALCULATION

The measured transformer power losses comprise core loss, winding loss, and stray loss, which cannot be easily separated by means of the measurement itself. To gain insight of the constitution and the spatial distribution of the power losses, finite element (FE) models were developed. A two-dimensional (2D) FE model was developed to investigate the core loss and the magnetising current; a three-dimensional (3D) FE model was used to calculate the stray loss (eddy current loss). The geometry of the 2D and 3D models are shown in Figure 8.

The magnetisation characteristic (Figure 9) of the magnetic core was obtained using the approach described in Section 2.2. In normal operation as well as in our test, the leakage flux density is too small to saturate the tank and the clamping plate. Therefore, constant relative permeability (100) was used for the iron tank and the clamping plate (mild steel). The conductivity was 6.99 mS/m.

Transient analyses considering non-linear magnetic properties often require significant computational efforts to obtain steady state solutions. When the problem involves a dc signal, the time constant for reaching steady state, determined by the ratio between the inductance and dc resistance of the winding, becomes extremely large. To deal with such a situation, the time periodic finite element method (TPFEM) [16] and the harmonic balance finite element method (HBFEM) [17] have been proposed. A comparison of the methods is given in [18]. Here, we used 2D TPFEM to calculate magnetising currents and core loss.

The governing equations in terms of a magnetic vector potential $\vec{A}$ is given by

$$\nabla \times \vec{H} + \sigma \frac{\partial \vec{A}}{\partial t} = \vec{J}_e \tag{2}$$

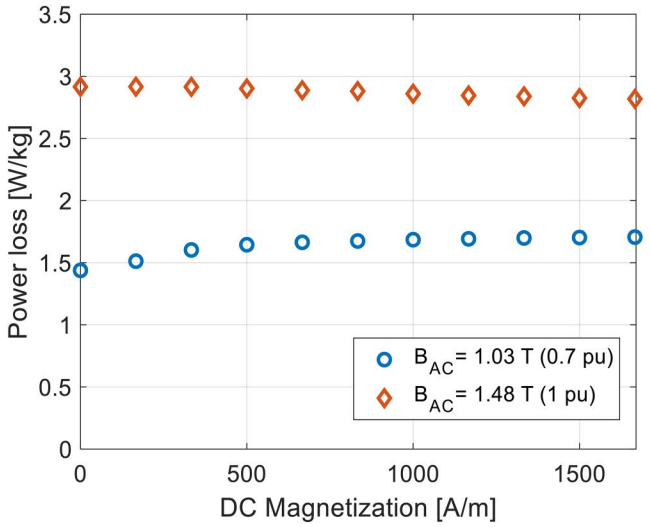

FIGURE 7 Measured specific power loss versus dc magnetisation. Red: nominal ac flux density (1 pu); Blue: low ac flux density (0.7 pu)

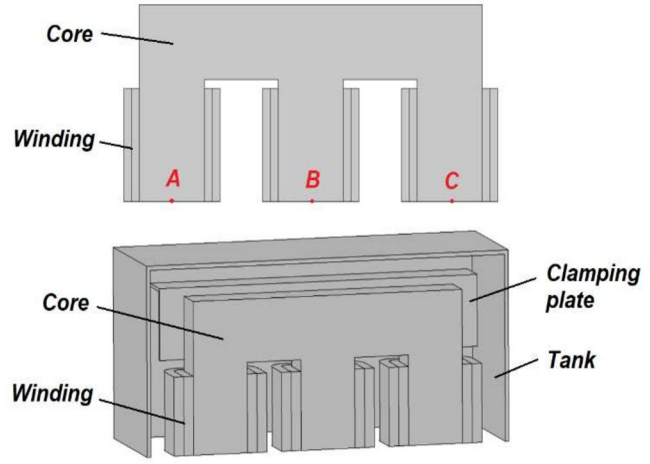

FIGURE 8 Views of the geometry of the FE models. Upper: 2D FE (half) model for core loss calculation. Lower: 3D FE (quarter) model for stray loss calculation

where σ is the conductivity of the material. $\overrightarrow{J}_e$ is the periodic excitation current density. When voltage sources are involved (e.g. in 2D FE models), the current density satisfies

$$\overrightarrow{J_e} = -\sigma\left(\frac{\partial \vec{A}}{\partial t} + \nabla \varnothing\right) \tag{3}$$

where Φ is the electric scalar potential related to the applied voltage sources.

Since saturation is included in the field problem, the magnetic field strength $\vec{H}$ is a non-linear function of the flux density $\vec{B}$

$$\vec{H} = \vec{H}\left(\vec{B}\right) = \vec{H}\left(\nabla \times \vec{A}\right) \tag{4}$$

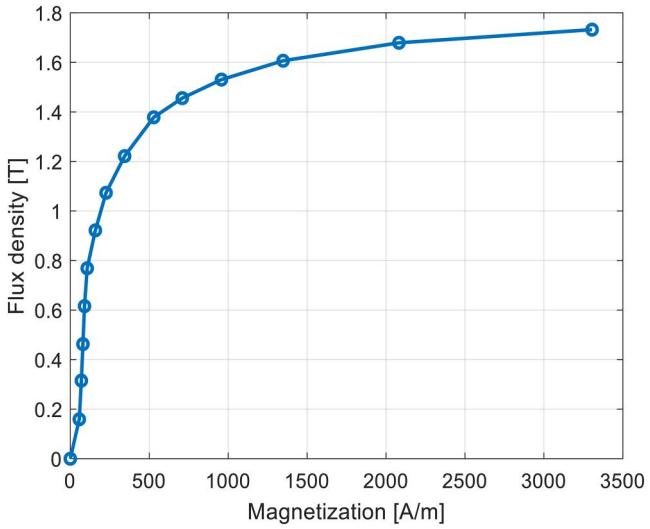

FIGURE 9 Measured magnetisation characteristic (B-H curve) for the transformer core

To implement TPFEM with commercial simulation codes (COMSOL Multiphysics®), the time domain Equation (2) is discretised into multiple coupled stationary problems:

$$\nabla \times \vec{H}\left(\nabla \times \overrightarrow{A_i}\right) + \sigma \frac{\overrightarrow{A_i} - \overrightarrow{A_{i-1}}}{2\frac{T}{N}} = \overrightarrow{J_{e,i}}\,|_{t=\frac{i}{N}T} \tag{5}$$

where T is the period of the excitation and N is the number of the time steps. $\overrightarrow{A}_i$ and $\overrightarrow{J}_{e,i}$ are the vector potential and excitation current at time step i. Equation (5) represents i discrete equations at specified time instants. A total of 40 points was used in one period in the study.

For the boundary conditions, the symmetric plane (the bottom plane in Figure 8) of the model is defined as a perfect magnetic conductor (i.e. no tangential magnetic field)

$$n \times \vec{H} = 0 \tag{6}$$

Magnetic insulation is defined for the vertical symmetric plane in the 3D model, as well as for the outer boundary of the whole study region

$$n \times \vec{A} = 0 \tag{7}$$

By integration of Equation (3) over the whole coil cross-section and by expressing the electric scalar potential explicitly by means of applied voltage, a set of ordinary differential equations are obtained (following the similar discretisation approach as in Equation 5)

$$N_t \cdot \overrightarrow{J_{e,i}} - \left[V_{\mathrm{dc}} + V_m \cdot \sin\left(2\pi \frac{i-1}{N}\right)\right] \cdot \frac{\sigma}{2l} + N_t \cdot \frac{\sigma}{2} \frac{\int\left(\overrightarrow{A_i} - \overrightarrow{A_{i-1}}\right) ds}{2\frac{T}{N}} = 0 \tag{8}$$

where N_t is the number of the turns, l is the out-of-plane depth, and V_{dc} and V_m are the dc voltage offset and the ac voltage amplitude applied, respectively.

With such implementation, the computation time is significantly reduced. When the flux density distribution is obtained, a post-processing approach is adopted to calculate power loss, based on the material measurements made for the *P-B* relationship, see Figures 5 and 7.

For stray loss analyses involving asymmetric or irregular geometries such as the tank and the clamping plate, 3D modelling must be applied. In 3D FE transient simulations, the obtained magnetising currents are defined as the current excitations [19]. Compared with the voltage source implementation, this requires significantly less memory and thereby saves computation time.

4 | RESULTS AND DISCUSSION

4.1 | Influence of the dc-bias on core loss

Ac nominal voltage (230 V) was applied on the primary winding, where the CM dc currents varied up to 4 A and the DM dc currents varied from 0.4 to 1.6 A. In the tests, the tank and clamping plates were disassembled such that the total power loss only consisted of core loss and winding loss (without stray loss from structural parts). The winding loss was derived from the obtained current and the winding resistance, whereas the core loss was obtained by withdrawing the winding loss from the total power loss.

The test results are presented in Figure 10 (CM dc current) and Table 2 (DM dc current for the four cases in Table 1). The total power loss due to CM currents increased with the dc current. The winding loss dominated the loss increment, whereas the core loss remained practically constant.

A similar behaviour was observed for DM, with the core loss remaining practically constant (with a maximum difference of 2.5%) as dc current increased. However, the winding loss of DM was significantly larger than that of CM at the same dc current level. Among the four different cases in DM, the 0° case gave the highest winding loss, although the difference was small.

Figure 11 shows the measured and calculated primary currents (magnetising currents) for the four DM cases. For comparison, the magnetising current under CM dc current of the same level (1.6 A) is presented. The simulated currents were in good agreement with the measured ones. Due to the ungrounded connection, the sum of the three currents in DM was zero. Although the dc component of the currents was the same (1.6 A), the peak (or harmonic contents) of the DM magnetising currents was significantly larger than that for CM, and thereby induced higher winding loss. Among the four cases in DM, the 0° case gave the highest peak magnetising current (at Phase A) and consequently the highest winding loss.

Figure 12 shows the maximum flux densities in the transformer core. The maximum flux densities are distributed differently in the three limbs for the four DM cases. The calculated flux density offsets at the centre of the limbs (at Points A, B, C specified in Figure 8) as well as the calculated core loss are presented in Table 3. The maximum flux densities of DM were significantly higher than those of CM. This difference is due to the fact that the DM flux can close its path inside the core, yielding a smaller reluctance path for the dc flux of DM and a higher flux density offset, whereas the CM flux must close its path outside the core, resulting in a much larger reluctance path and a small flux density offset.

The higher flux densities (or flux density offsets) did not lead to higher core loss. On the contrary, the core loss slightly reduced (Table 2) due to the dc-bias. Despite decreased core loss, the dc-bias produced higher magnetising current and higher winding loss.

The magnetic core in the test transformer is made of isotropic material. As seen from Figure 12, the flux density is not uniform in the corner and joint regions. When anisotropic material (e.g. grain-oriented steel) is used, the flux density would be more uniform throughout the core. More importantly, grain-oriented material often has a much steeper magnetisation curve, which indicates less flux density offset but higher magnetisation current peak under saturation. Therefore, the current harmonic, winding loss and the stray loss are expected to be more pronounced.

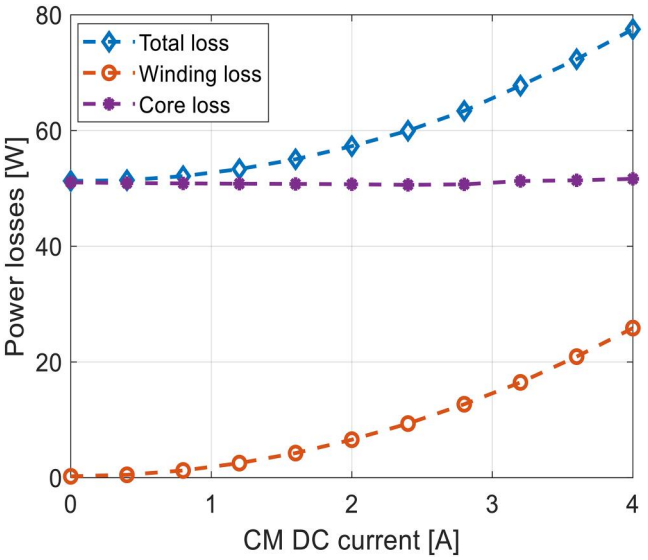

FIGURE 10 Power losses versus dc-bias of CM. The dashed lines are guides to the eye

TABLE 2 Winding losses and core losses due to the dc-bias of DM

	Winding loss (W)				Core loss (W)			
DC current (A)	0°	60°	90°	150°	0°	60°	90°	150°
0.4	0.79	0.79	0.79	0.74	50.0	49.5	49.7	49.8
0.8	2.30	2.16	2.18	2.16	49.8	49.6	49.5	49.5
1.2	4.62	4.28	4.39	4.32	49.5	49.6	49.4	49.1
1.6	7.70	7.13	7.35	7.29	49.3	49.7	49.4	48.8

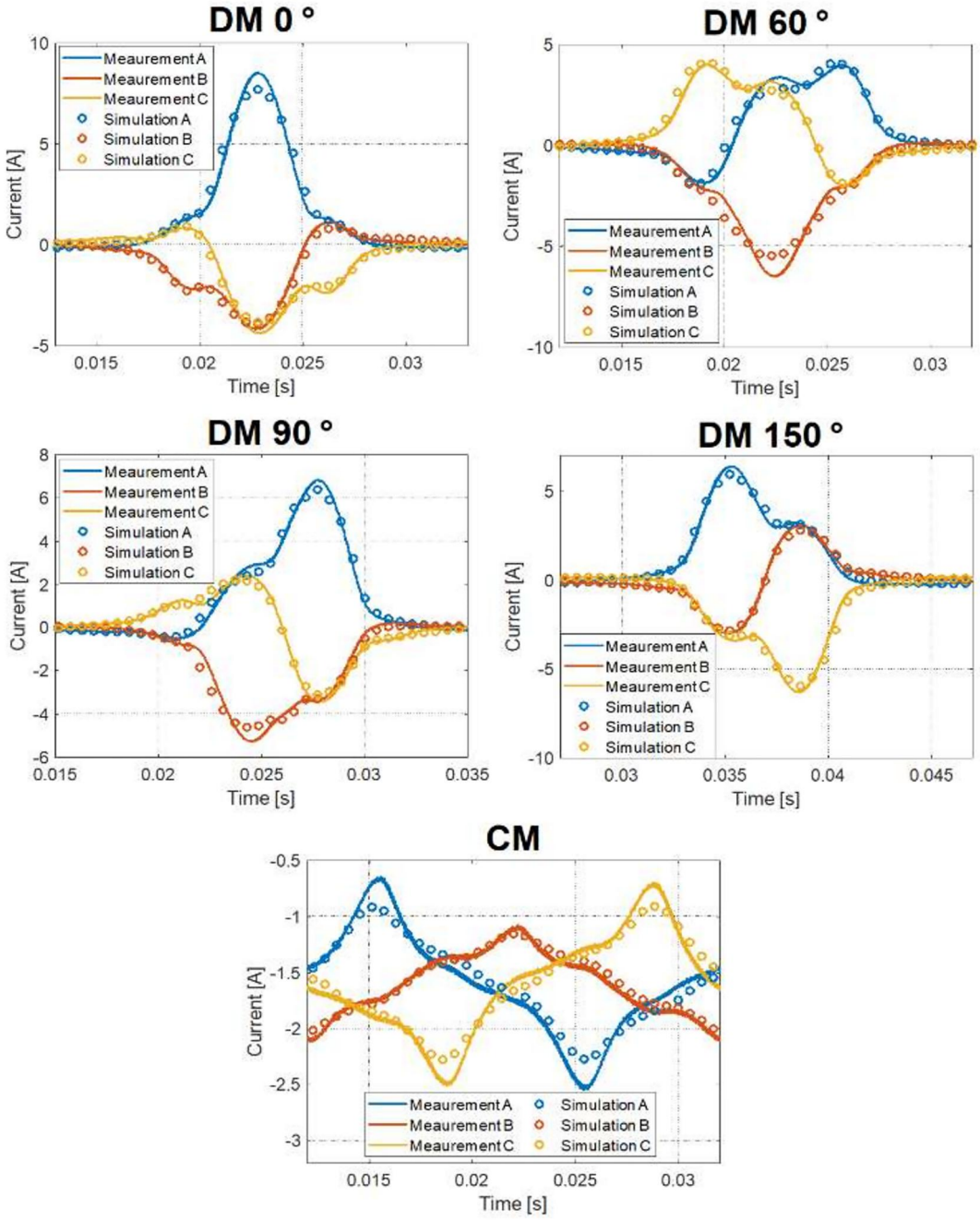

FIGURE 11 Comparison of the measured and calculated primary phase currents over one period at 1.6 A dc current for the four different DM cases and for the CM case. A, B, and C refer to the different positions given in Figure 8

4.2 | Influence of the dc-bias on stray loss

For stray loss investigations, the structural parts were included. The structural parts were added in two steps. First, only the iron tank was added (i.e. the clamping plates were excluded). In this case, the total power loss consisted of core loss, winding loss and the stray loss from the tank. The same ac voltage and dc currents were applied as in Section 4.1, and the winding loss was derived again from the obtained current. As the excitation maintained the same, the core loss was assumed to be identical to the case without the clamping plate (Section 4.1). Thus, the stray loss could be estimated by withdrawing the winding and core losses from the total loss.

The test results at 1.2 A are presented in Table 4. Both stray loss and winding loss were significantly higher for DM than for CM. The magnetising currents as well as the winding losses remained virtually unchanged when the tank was added. The stray loss differed considerably between the four DM cases, where the 60° case gave the highest loss. The simulated stray loss (i.e. eddy current loss in the tank) waveform over one

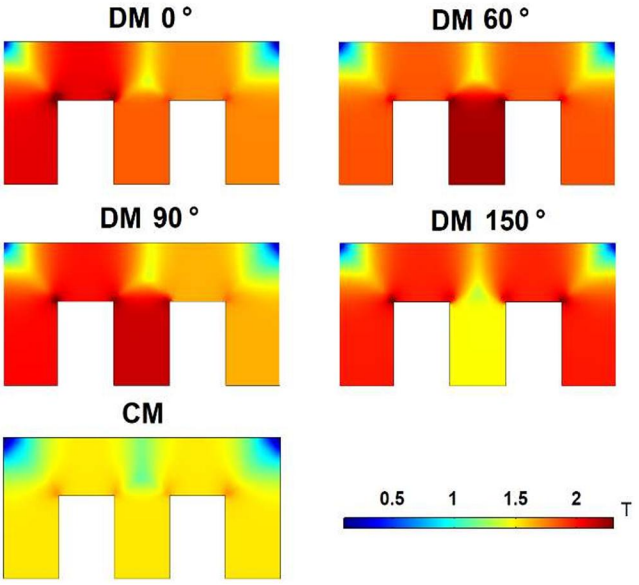

FIGURE 12 The maximum flux density in the magnetic core at 1.6 A dc current for the four DM and the CM cases

TABLE 3 Comparison of flux density offset and core losses due to DC-bias of DM and CM

Mode	θ	Calculated flux density offset in the middle of each limb (T) ΔB_A	ΔB_B	ΔB_C	Core loss (W) P_c
DM	0°	0.61	0.36	0.26	49.4
	60°	0.38	0.75	0.38	49.5
	90°	0.54	0.66	0.14	49.4
	150°	0.51	0	0.51	49.4
CM	/	0.01	0.01	0.01	50.1

TABLE 4 Comparison of power losses with 1.2 A DC-bias in DM and CM

Mode	θ	Measured losses (W) Total loss	Winding loss	Stray loss	Calculated stray loss (W)
DM	0°	59.3	4.5	5.6	6.0
	60°	62.5	4.3	8.6	8.0
	90°	61.4	4.3	7.7	7.0
	150°	58.2	4.3	5.2	5.4
CM	/	52.9	2.5	0.3	0.3

Abbreviations: CM, common mode; DM, differential mode.

period is presented in Figure 13 and the calculated average values are listed in the last column in Table 4. The difference between the calculated stray losses and the measurement likely

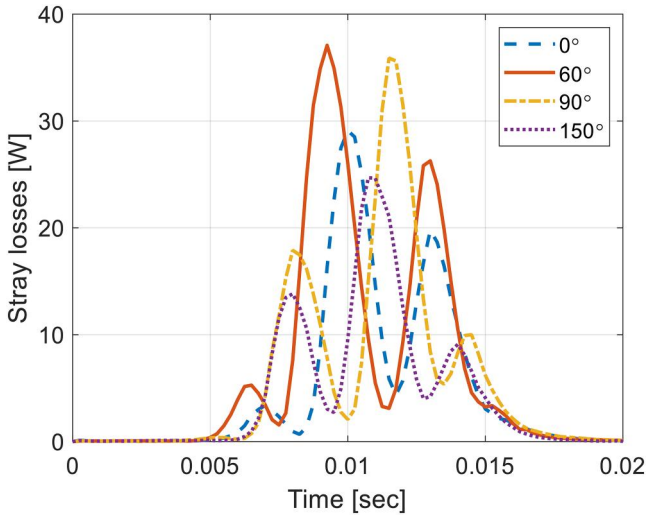

FIGURE 13 The instantaneous stray loss in the iron tank under 1.2 A DM dc current for the four cases. The 0.02 s corresponds to one period

attributes to the neglected geometrical details, such as slots and holes (Figure 3) in the numerical modelling.

Figure 14 shows the maximum stray loss density distribution in the tank for the four cases. The symmetry/asymmetry of the flux density distribution within the core limbs determines the symmetry/asymmetry distribution of the induced stray losses in the tank. For example, at 60° and 150°, the flux density is symmetric with respect to the centre limb (see Figure 12) and so is the loss density (Figure 14). In contrast, at 0° and 90°, the loss concentrates on one side of the tank due to the asymmetric flux density distribution. Among the four cases, the 60° case has the highest magnitude of the loss density, and generates the maximum stray loss.

In the next step, the complete transformer unit was measured (i.e. both tank and clamping plates were included). The stray loss and the winding loss are presented in Figure 15. By including the clamping plates, the stray loss significantly increased. There is a large difference in stray loss between the four DM cases, particularly at higher dc-bias levels. In contrast, the winding losses are almost the same for the four cases.

The stray loss variation and distribution is given for the 60° case in Figure 16. By adding the clamping plates, the total stray loss is increased not only by the added clamping plates, but also by the incremental stray loss in the tank, due to the reduced clearance between the tank and the core. The stray loss of the clamping plates concentrated on the edges close to the winding terminals. The loss concentration area presented in Figures 14 and 16 also indicates the location where the mitigation measures such as a magnetic shunt shall be placed.

4.3 | Influence of delta winding

To evaluate the influence of the delta winding, measurements were made with the secondary winding in delta configuration

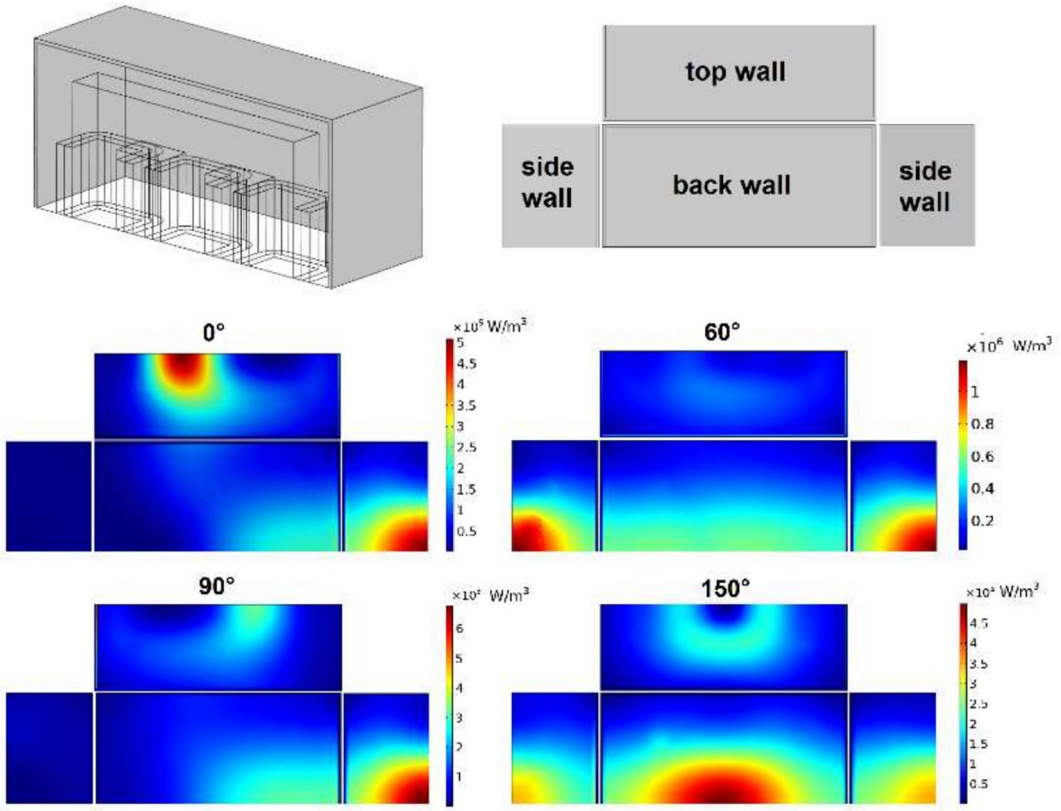

FIGURE 14 The maximum volumetric stray loss density in the tank at 1.2 A DM dc current for the four cases. The upper left figure shows a 3D view of the tank and the upper right figure shows how the tank walls are expanded in a 2D view. One quarter of the model is shown

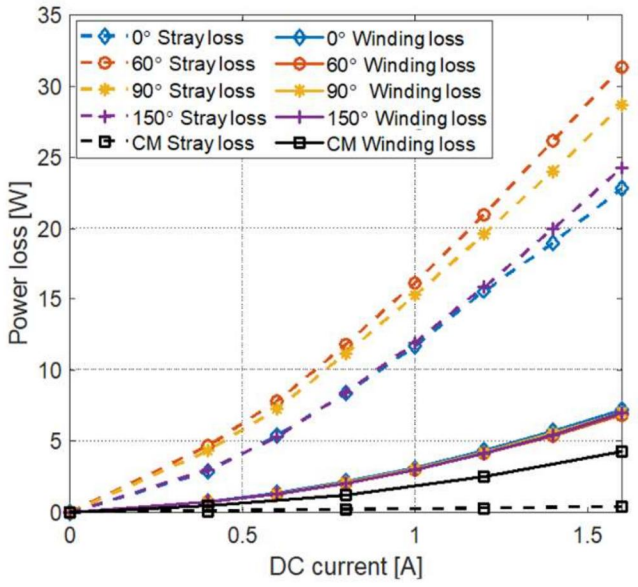

FIGURE 15 Stray loss and winding loss (with both tank and clamping structure) due to DM dc current for the four different cases. For comparison, stray loss and winding loss due to CM are also included

(closing the switch in Figure 2). The stray loss as well as the winding loss at a dc current of 1.6 A are presented in Table 5. As for the previous cases, the winding loss was derived from the measured current, and the stray loss was estimated by withdrawing the winding loss and the core loss from the total loss.

The delta winding connection resulted in dramatically reduced stray loss (Table 5 compared with Table 4) caused by the dc-bias with the cost of only the modest additional loss in the secondary winding. In addition, the loss difference between the four cases greatly reduced. The simulated example, Figure 17, is given for the 0° case, showing the reduced instantaneous loss with delta winding.

The circulating current in the delta winding was also calculated in the FE analyses, and it was in good agreement with the recorded measured waveform, see Figure 18. The (induced) circulating current counteracted the leakage field generated by the magnetising current, and thereby reduced the stray loss.

5 | DISCUSSION

Traditionally, mitigation measures can be classified into prevention of the creation of GICs and prevention of the transformer core from saturation [20]. The former strategy includes line connected methods [21] and neutral dc blocking devices [22]. For example, a fundamental frequency-blocking filter is used to reduce the fundamental current in the transmission line from inductive coupling, and thereby reduces dc current. A series capacitor can be used to block GICs on line. However, the

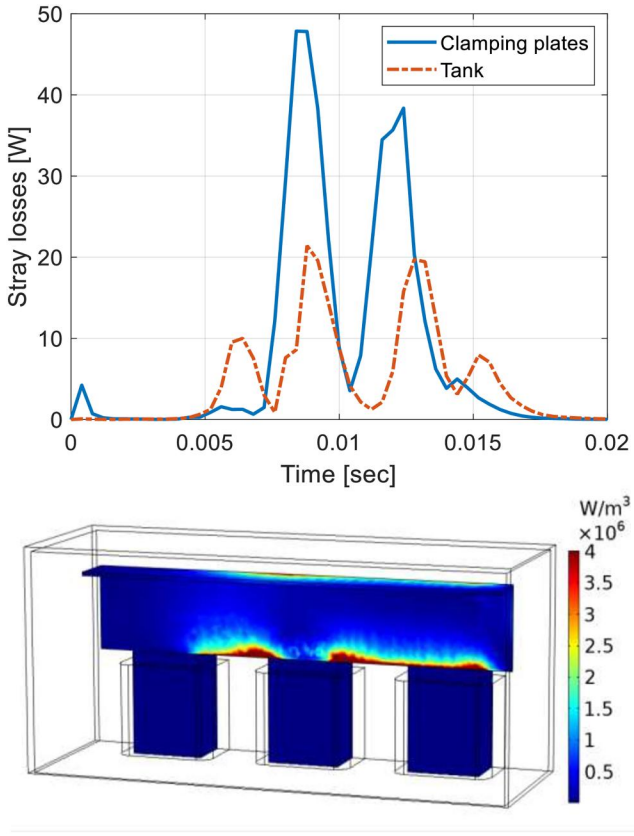

FIGURE 16 The calculated stray loss under DM dc current of case 60°. Upper: the instantaneous stray loss over one period in the tank and the clamping plates. Lower: the maximum volumetric stray loss density in the clamping plates

TABLE 5 Power losses due to DC-bias in DM with delta winding

		Measured power losses (W)		
Mode	***θ***	**Stray loss**	**Primary winding loss**	**Secondary winding loss**
DM	0°	1.1	4.7	0.6
	60°	0.9	4.4	1.1
	90°	0.9	4.4	0.9
	150°	0.5	4.3	0.5

line connected methods often involve line insulation level and high equipment costs. In contrast, neutral dc blocking devices require much lower voltage rating and less investment. For the counter-saturation strategy, it often suggests using three-phase three-limb transformers to increase reluctance of dc flux [3].

However, for DM dc current, our study shows that the saturation phenomenon is also significant in a three-phase three-limb transformer and that the stray loss can be substantial. Moreover, the neutral blocking device is not a feasible solution since the DM dc current circulates within three phases. Fortunately, most large three-phase transformers used in HVDC link are equipped with delta winding. As discussed in Section 4.3, the

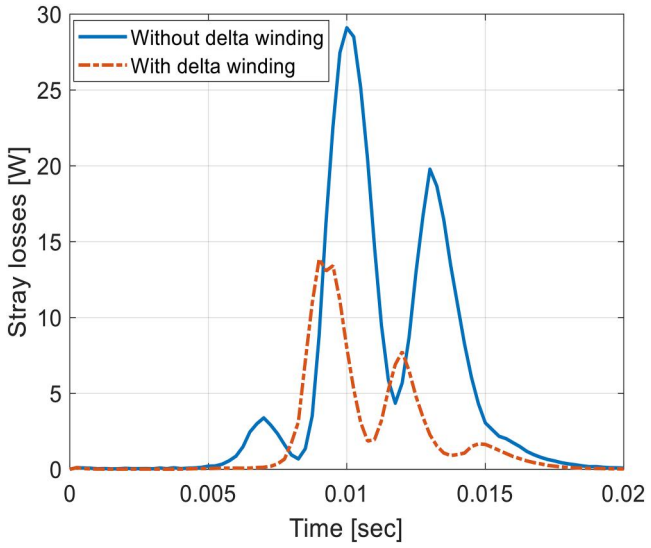

FIGURE 17 The calculated instantaneous stray loss over one period in the tank under 1.2 A DM dc current for the 0° case

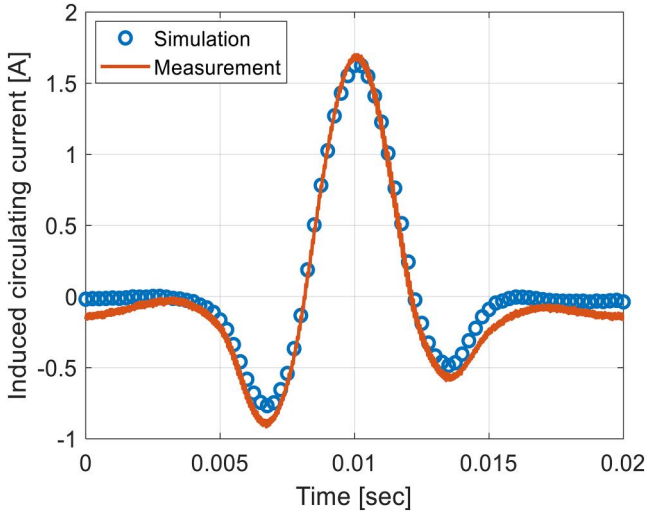

FIGURE 18 Comparison between the calculated circulating current in the delta winding and the measurement over one period in the tank under 1.2 A DM dc current for the 0° case

stray loss can be largely reduced if delta winding exists and proper rating is considered. Otherwise, line connected devices or the control compensation method [23] shall be considered.

6 | CONCLUSIONS

The experimental and modelling study revealed significantly different behaviour in terms of power loss between CM and DM as well as between four DM cases.

- The flux density offset (as well as the maximum flux density) due to DM dc-bias was significantly larger than that in CM (Figure 12 and Table 3), due to the low reluctance path in

DM. Among the four cases, 60° gave the highest offset and thereby the worst case.

- The core loss was not sensitive to dc-bias, regardless of the magnitudes and modes of the applied dc currents (Figure 10 and Table 3).
- The winding loss due to DM dc-bias was significantly larger than that of CM (Table 4 and Figure 15), due to high magnitudes of the magnetising currents as well as their high frequency harmonic contents. For the winding loss, there were only small differences between the different cases.
- The stray losses differed between the four DM cases, where 60° gave the highest loss and 150° gave the lowest loss (Figure 15). The geometry of the tank and the clamping had a dramatic impact on the stray loss.
- The excessive stray loss caused by the DM dc currents was reduced significantly by introducing delta winding (Table 5 and Figure 17).

The results above shows that a three-phase three-limb transformer, which is vulnerable to CM dc currents, is susceptible to DM dc current. The DM dc-bias can constitute a local overheating hazard in the tank and the clamping plates in a power converter connected transformer, particularly if delta winding is not used.

ACKNOWLEDGEMENTS

This work was performed as a part of the project 'Thermal Modelling of Transformers' (Norges Forskningsråd project no.: 255178) funded by the Research Council of Norway, Statnett, Hafslund, and Lyse Nett.

CONFLICT OF INTERESTS

The authors declare that there are no conflict of interests.

DATA AVAILABILITY STATEMENT

The data that support the findings of this study are available from the corresponding author upon reasonable request.

ORCID

Wei Wang https://orcid.org/0000-0001-6413-2449

REFERENCES

1. Pirjola, R.: Geomagnetically induced currents during magnetic storms. IEEE Trans. Plasma Sci. 28(6), 1867–1873 (2000). https://doi.org/10.1109/27.902215
2. Jiang, Y., Ekström, A.: General analysis of harmonic transfer through converters. IEEE Trans. Power Electron. 12(2), 287–293 (1997). https://doi.org/10.1109/63.558741
3. IEEE guide for establishing power transformer capability while under geomagnetic disturbances, IEEEC57.163 (2015)
4. Price, P.R.: Geomagnetically induced current effects on transformers. IEEE Trans. Power Del. 17(4), 1002–1008 (2002). https://doi.org/10.1109/TPWRD.2002.803710
5. Gattens, P., Waggel, R.M.: Investigation of transformer overheating due to solar magnetic disturbances. IEEE Special Panel Session Report (1989)
6. Bozoki, B., et al.: The effects of GIC on protective relaying. IEEE Trans. Power Del. 11(2), 725–739 (1996). https://doi.org/10.1109/61.489329
7. NERC report: March 13, 1989 geomagnetic disturbances. http://www.nerc.com/files/1989-Quebec-disturbance.pdf (1990). Accessed 20 Aug 2020
8. Larsen, E.V., Walling, R.A., Bridenbaugh, C.J.: Parallel AC/DC transmission lines steady-state induction issues. IEEE Trans. Power Del. 4(1), 667–674 (1989). https://doi.org/10.1109/61.19259
9. Ulleryd, J., Ye, M., Moreau, G.: Fundamental frequency coupling between HVAC and HVDC lines in the Quebec-New England multiterminal system-comparison between field measurements and EMTDC simulations, In: International Conference on Power System Technology, 498–502 (1998). https://doi.org/10.1109/ICPST.1998.729013
10. Vestergaard, O., Lundberg, P.: Maritime link the first bipolar VSC HVDC with overhead line. In: AEIT HVDC International Conference, pp. 1–4. (2019). https://doi.org/10.1109/AEIT-HVDC.2019.8740513
11. Sagstad, T.: Power solutions for Johan Sverdrup field in phase 1 and for full field. Technical Report, Statoil, RE-PM312-00137. Rev. 1 (2014)
12. Wang, W., Nysveen, A., Magnusson, N.: Common and differential mode of dc-bias in three-phase power transformer (2021)
13. Magnetic materials-part 2: methods of measurement of the magnetic properties of electrical steel strip and sheet by means of an epstein frame. IEC 60404-2 (2008)
14. Magnetic materials-part 3: methods of measurement of the magnetic properties of electrical steel strip and sheet by means of a single sheet tester. IEC 60404-3 (2009)
15. Wang, W., Nysveen, A., Magnusson, N.: Apparatus for loss measurements under multidirectional and dc-bias flux in electrical steel laminations. Rev. Sci. Instrum. 91, 084705 (2020)
16. Takahashi, Y., et al.: Parallel time-periodic finite-element method for steady-state analysis of rotating machines. IEEE Trans. Magn. 48(2), 1019–1022 (2012). https://doi.org/10.1109/TMAG.2011.2171923
17. Yamada, S., Bessho, K.: Harmonic field calculation by the combination of finite element analysis and harmonic balance method. IEEE Trans. Magn. 24(6), 2588–2590 (1988). https://doi.org/10.1109/20.92182
18. Ausserhofer, S., Biro, O., Preis, K.: Frequency and time domain analysis of nonlinear periodic electromagnetic problems. In: International Conference on Electromagnetics in Advanced Applications (2007). https://doi.org/10.1109/ICEAA.2007.4387279
19. Ngnegueu, T., et al.: Behaviour of transformers under DC/GIC excitation: Phenomenon, impact on design/design evaluation process and modelling aspects in support of design. CIGRE Session, A2-303 (2012)
20. Mousavi, S.A.: Electromagnetic modelling of power transformers for study and mitigation of effects of GICs. Dissertation, Royal Institute of Technology (2015)
21. Marti, L.: Effects of series compensation capacitors on geomagnetically induced currents. IEEE Trans. Power. Del. 29(4), 2032–2033 (2014)
22. Wang, Z., et al.: Novel DC bias suppression device based on adjustable parallel resistances. IEEE Trans. Power. Del. 33(4), 1787–1797 (2018)
23. Trinh, Q.N., Peng, W., Hoong, C.F.: Elimination of DC and harmonic current injection due to grid voltage measurement errors in three-phase grid-connected inverter. In: IEEE 3rd International Future Energy Electronics Conference and ECCE Asia, pp. 894–899. (2017)

How to cite this article: Wang, W., Nysveen, A., Magnusson, N.: Power losses in the three-phase three-limb transformer due to common and differential mode of dc-bias. IET Electr. Power Appl. 1–11 (2021). https://doi.org/10.1049/elp2.12113